Journal of Materials Chemistry C

Degradable semiconducting polymers without long-range order for on-demand degradation of transient electronics

Journal:	*Journal of Materials Chemistry C*
Manuscript ID	TC-ART-08-2023-003079.R1
Article Type:	Paper
Date Submitted by the Author:	11-Oct-2023
Complete List of Authors:	Chiong, Jerika; Stanford University, Chemistry Michalek, Lukas; Stanford University, Chemical Engineering Pena-Alcantara, Amnahir; Stanford University, Materials Science and Engineering Schuster, Nathaniel; Stanford University, Chemical Engineering Ji, Xiaozhou; Stanford University, Chemical Engineering Bao, Zhenan; Stanford University, Chemical Engineering; Stanford University, Chemistry

ARTICLE

Degradable semiconducting polymers without long-range order for on-demand degradation of transient electronics

Received 00th January 20xx,
Accepted 00th January 20xx

DOI: 10.1039/x0xx00000x

Jerika A. Chiong,[a,b] Lukas Michalek,[b] Amnahir E. Peña-Alcántara,[c] Xiaozhou Ji,[b] Nathaniel J. Schuster,[b] and Zhenan Bao[a,b,*]

Current understanding of molecular design principles for degradable imine-based polymer semiconductors is limited to semicrystalline polymer morphologies. Herein, we design and synthesize a new class of degradable, nanocrystalline semiconducting polymers based off of indacenodithiophene (IDT) units using less toxic methods compared to commonly-used Stille polycondensation. Through the lack of long-range order of the degradable IDT-based polymer films, we show that enhanced stretchability can be achieved while maintaining similar electronic performance to their degradable, semicrystalline diketopyrrolopyrrole (DPP)-based counterpart. Degradation studies by ultraviolet-visible spectroscopy, gel permeation chromatography, nuclear magnetic resonance spectroscopy, and quartz crystal microbalance reveal the IDT-based polymers degrade orders of magnitude faster than the semicrystalline DPP-based polymer (within hours in solution and within one week in the thin film). Moreover, the IDT-based polymers can be degraded in milder acidic conditions (0.1 M HCl) than those used for semicrystalline DPP-based polymers, resembling acidic environments in the human body and allowing for environmentally-friendlier conditions from synthesis to degradation. Our work strengthens our understanding of structure-degradation property relationships of polymer semiconductors and paves the way toward transient electronics with triggerable, on-demand degradation.

1. Introduction

In recent years, polymer-based semiconductors have garnered attention for their use in transient electronics that interface with the human body and environment.[1–8] Such electronic devices have applications for implantable biomedical diagnostics,[9–11] secure and traceless materials,[12–14] and the reduction of hazardous electronic waste in landfills and impoverished communities.[15–17] Currently, high-performing, degradable semiconducting polymers require toxic reagents for synthesis as well as harsh acidic conditions for degradation, preventing use in physiologically and environmentally-relevant applications.[3,5,6] In order for integration with healthcare and the environment, these semiconductors need to maintain reasonable electronic performance while being able to degrade under biologically benign conditions, motivating the need for greener syntheses and novel polymer design.

Previously, we studied the impact of sidechain engineering parameters on the degradation lifetimes of diketopyrrolopyrrole (DPP)-based semiconducting polymers.[6] Unlike traditional degradable polymers for plastics, these donor-acceptor (D-A) conjugated polymers had relatively long degradation times even under harsh acidic conditions (e.g., 0.5 M trifluoroacetic acid) due to their hydrophobic nature and strong aggregation in both solution and thin film.[6] In order to design semiconducting polymers with both good charge transport and shorter degradation timescales under ecologically-friendlier conditions, we look to new polymer backbones to tune morphological parameters to a greater degree. The D-A conjugated polymer indacenodithiophene-co-benzothiadiazole (pIDT-BT) is known to have high charge carrier mobilities despite its "disordered" morphology, or one that lacks long-range order, due to its planar, rigid backbone stabilized by non-covalent interactions between the indacenodithiophene (IDT) and benzothiadiazole (BT) units.[18–26] Inspired by pIDT-BT, we aim to design a new class of degradable, nanocrystalline imine-based semiconducting polymers with degradation kinetics that differ from that of their degradable, semicrystalline DPP-based polymer counterparts. The synthesis and characterization of such polymers will further the understanding of the molecular structure-degradation property relationships of imine-based conjugated polymers. Based on previous understanding of the influence of aggregation on degradation lifetimes,[6] we hypothesize that unlike semicrystalline polymer semiconductors, these planar but more amorphous polymers will maintain good charge transport while allowing for accelerated degradation timescales due to their lack of long-range order and crystallinity (Figure 1a).

Herein, we prepare degradable IDT-based semiconducting polymers by incorporating acid-cleavable imine bonds into the polymer backbone to impart degradability while flanking them with BT units to maintain backbone planarity. Two degradable pIDT-BT

[a]Dept. of Chemistry, Stanford University, Stanford, CA 94305, USA
[b]Dept. of Chemical Engineering, Stanford University, Stanford, CA 94305, USA
[c]Dept. of Materials Science and Engineering, Stanford University, Stanford, CA 94305, USA

† Electronic Supplementary Information (ESI) available: Detailed synthetic procedures, NMR, DFT and TD-DFT calculations, additional UV–vis spectra, PESA, GIXD line profiles, AFM, crack onset strain, additional FET transfer and output curves, UV–vis degradation data, GPC degradation data, NMR degradation experiments, contact angle measurements, and QCM. See DOI: 10.1039/x0xx00000x

copolymer derivatives were designed and synthesized with differing electrostatic interactions and electronic properties (Figure 1b). Terpolymerization was employed to further tune the degradation behavior and electronic performance of these degradable IDT-based polymers. The nondegradable, nanocrystalline pIDT-BT and degradable, semicrystalline DPP- and thiophene-imine-thiophene (TIT)-based polymer pDPP-TIT were also synthesized as reference polymers. In order to examine the effect of the incorporated imine groups on backbone planarity and emergent properties of the degradable IDT-based polymers, we conducted density functional theory (DFT) calculations as well as characterized the polymers' optical and morphological properties by ultraviolet-visible (UV-vis) absorption spectroscopy, photoelectron spectroscopy in air (PESA), grazing-incidence X-ray diffraction (GIXD), and atomic force microscopy (AFM). Both the mechanical and electronic properties of the semiconductors were measured. Finally, degradation of the polymers was monitored and compared to that of the reference polymers (pIDT-BT and pDPP-TIT) by UV-vis, NMR, gel permeation chromatography (GPC), and quartz crystal microbalance (QCM). We observed that altering polymer backbone structures, and thus film morphologies, indeed affects degradation behavior to a greater extent than through sidechain engineering, facilitating faster degradation closer to environmentally-relevant conditions. Our results provide new insights toward designing polymer semiconductors that can degrade under biologically-friendly conditions for real-world applications of transient electronics.

2. Results and discussion

2.1. Synthesis of Degradable IDT-Based Polymers

Two degradable BT-based imine monomers were synthesized for copolymerization with commercially-available di(boron-pinacolato)-functionalized IDT. We designed a benzothiadiazole-imine-benzothiadiazole (BTiBT) monomer to mimic pIDT-BT and maintain backbone planarity as well as a benzothiadiazole-imine-phenyl (BTiPh) monomer to mitigate the effects of the additional electron-withdrawing imine and BT unit and examine the impact of structural differences on planarity. The synthetic routes toward dibromo-functionalized BTiBT and BTiPh (Br-BTiBT-Br and Br-BTiPh-Br) are outlined in Figure 2. Br-BTiBT-Br was synthesized in three steps, while Br-BTiPh-Br was synthesized in just one step from commercially-available materials. During imine formation, it was noted that Br-BTiBT-Br was less stable to hydrolytic cleavage than Br-

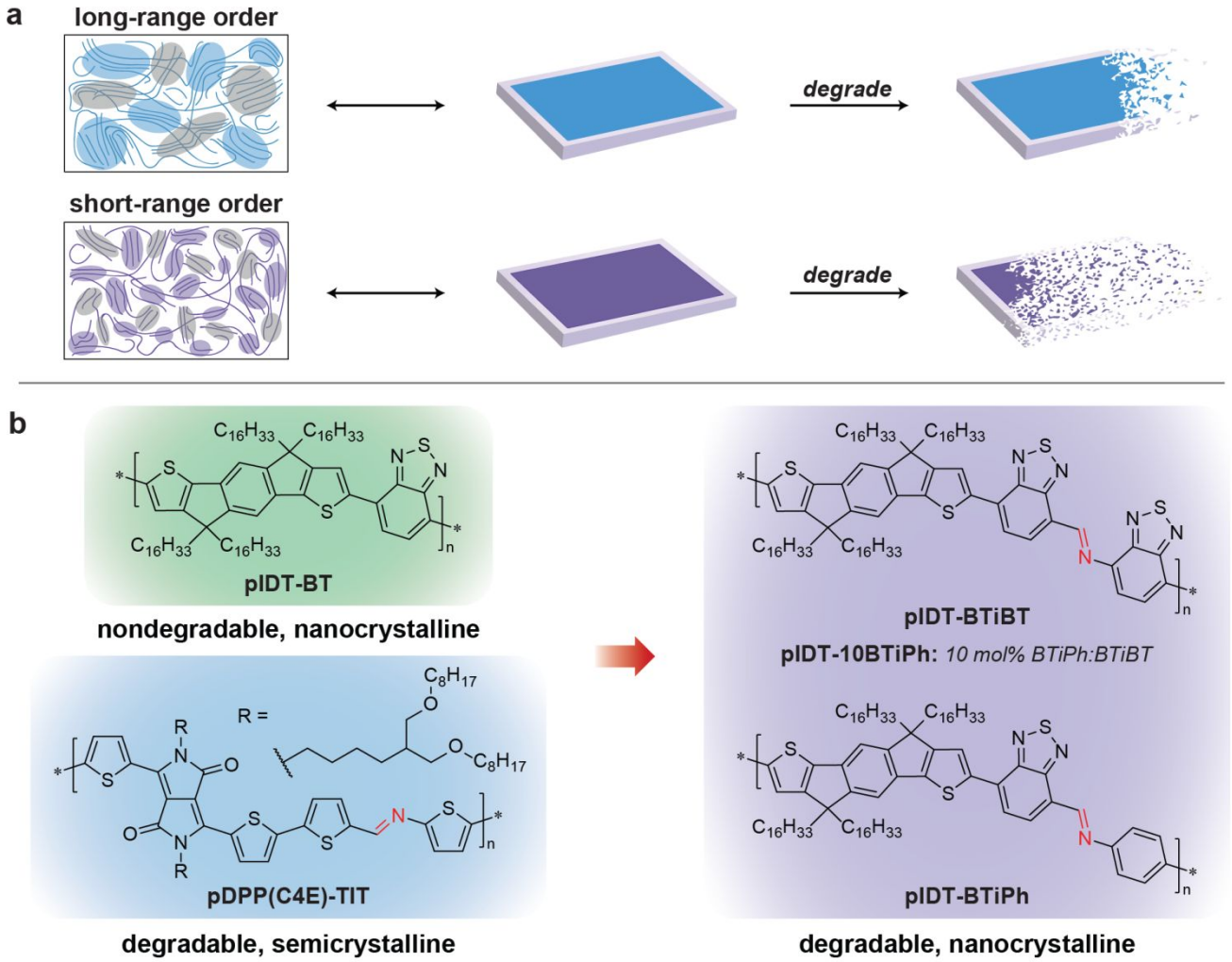

Figure 1. General schematic and molecular design of polymers in this study. (a) Degradable polymer semiconductors lacking long-range order are expected to degrade faster and under more biologically-friendly conditions compared to degradable, semicrystalline polymers due to their less crystalline morphology. (b) Design of several imine-based semiconducting polymers with short-range order inspired by nondegradable pIDT-BT[18] and degradable pDPP(C4E)-TIT.[6]

BTiPh-Br, requiring use of a drying agent (i.e., crushed molecular sieves). We hypothesize that the instability of the BTiBT monomer was likely due to the energetically less favorable imine formation as the imine was flanked by two strongly electron-withdrawing BT units, while the phenyl group in BTiPh stabilized the imine bond. Detailed synthetic procedures and characterizations are described in the Supporting Information (Figures S1-5).

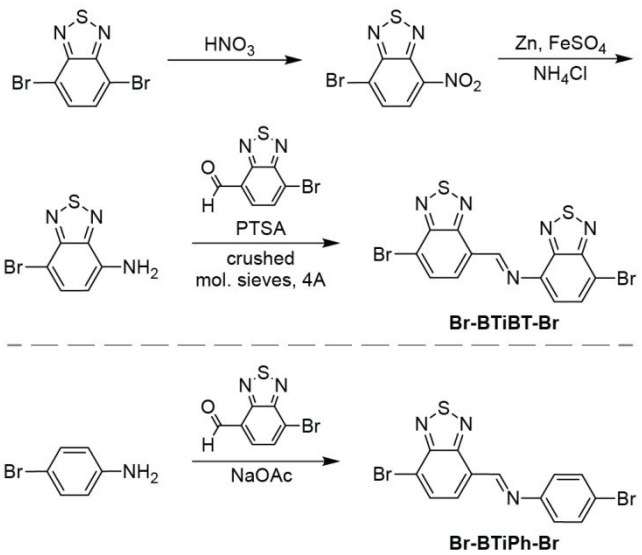

Figure 2. Synthetic schemes for the preparation of Br-BTiBT-Br and Br-BTiPh-Br monomers.

To forgo the use of toxic tin reagents in both monomer synthesis and polymerization for greener syntheses, we used Suzuki cross-couplings for polycondensation instead of commonly used Stille couplings. We prepared degradable IDT-based semiconducting polymers using the highly reactive XPhos Pd G3 catalyst for fast reaction to avoid deboronation of the electron-donating IDT monomer (Figures S6-11).[27] Due to the instability of Br-BTiBT-Br and use of water in Suzuki condensation polymerizations, relatively low M_n for pIDT-BTiBT was obtained (Table 1). These results suggest that the imine bond in Br-BTiBT-Br cleaves during polymerization, effectively end-capping the polymer chain. Higher M_n was achieved for the copolymerization of IDT and BTiPh monomers. To increase polymer M_n for improved mechanical and electronic properties while aiming to maintain backbone rigidity through stabilizing interactions between IDT and BT units,[28,29] we synthesized a terpolymer pIDT-10BTiPh using a 9:1 BTiBT:BTiPh monomer ratio. Reference polymers pIDT-BT and pDPP-TIT were synthesized with similar M_n according to literature procedures (Figures S12-13).[3,6,27] From our previous study, we selected pDPP-TIT with branched alkyl C4 spacer sidechains and ether functionalities (C4E) for comparison as this semicrystalline polymer degraded the fastest (within 10 days in solution treated with a 1000-fold molar excess of acid and water). It should be noted that due to the asymmetry of all imine-based monomers, polymerization by cross-couplings led to regiorandom polymers (Figure S14). The M_n, dispersity ($Đ$), and number-average degree of polymerization (DP_n) were determined by high-temperature GPC (HT-GPC) using trichlorobenzene as the solvent at 180 °C (Table 1).

Table 1. HT-GPC Characterization

polymer	M_n (kg/mol)	$Đ$	DP_n[a]
pIDT-BTiBT	9.5	2.0	6
pIDT-10BTiPh	11.5	2.1	8
pIDT-BTiPh	31.1	2.3	22
pIDT-BT	23.4	2.0	18
pDPP(C4E)-TIT	20.1	3.3	17

[a]Average molecular weight of the repeat units commensurate with the molar ratio of incorporation were used for pIDT-10BTiPh terpolymer.

For studying the degradation products of the degradable IDT-based semiconducting polymers, we synthesized IDT flanked by aldehyde-functionalized BT units through Suzuki cross-coupling for comparison (Figure S15). For ease of synthesis, we used this model degradation compound as an experimental reference for the mixture of degradation products and modeled the other products by time-dependent density functional theory (TD-DFT) calculations (*vide infra*).

2.2. DFT and TD-DFT Calculations

To examine the structural differences among pIDT-BT and our new degradable IDT-based polymers, we optimized the geometries of the synthesized degradable units flanked by thiophenes (to mimic IDT units) using DFT (at the B3LYP-D3/6-31G** level in the gas phase). A complete description of the calculations is provided in the Supporting Information. Based on reported understanding of stabilizing non-covalent interactions from the thiophene fragment of IDT with the BT unit, we positioned the BT and thiophene units in a "cis" orientation (with both thiophene sulfurs oriented toward the BT hydrogens) (Figure S16).[24,30] There are four different cis conformational isomers for BTiBT and two for BTiPh (Figures S17-18). From their optimized geometries, total Gibbs free energies and Boltzmann distributions (at 298.15 K) were calculated. For both BTiBT and BTiPh, the predominant conformations (predicted to be >94% of their conformational ensembles) were used for comparison, with the imine hydrogen pointed toward the nitrogen on the neighboring BT unit due to potential hydrogen bonding interactions (Table S1 and Figure S19).

Comparing geometries of the most energetically-favored conformer for BT, BTiBT, and BTiPh with neighboring thiophenes (T), T-BT-T was the most planar followed by T-BTiBT-T then T-BTiPh-T (Figure 3). While the dihedral angles between thiophenes and BT units were 0° on both sides in T-BT-T, suggesting pIDT-BT was completely planar and rigid, the T-BTiBT-T fragment was slightly twisted out of plane (dihedral angles of <10°). In contrast, the T-BTiPh-T unit showed more significant twisting with the phenyl group being rotated ~30° on either side. Based on these calculations, we expect degradable pIDT-BTiBT to deviate slightly from traditional pIDT-BT morphology, whereas pIDT-BTiPh should display an even less ordered and more amorphous morphology due to its backbone twisting. As p-type semiconductors, the highest occupied molecular

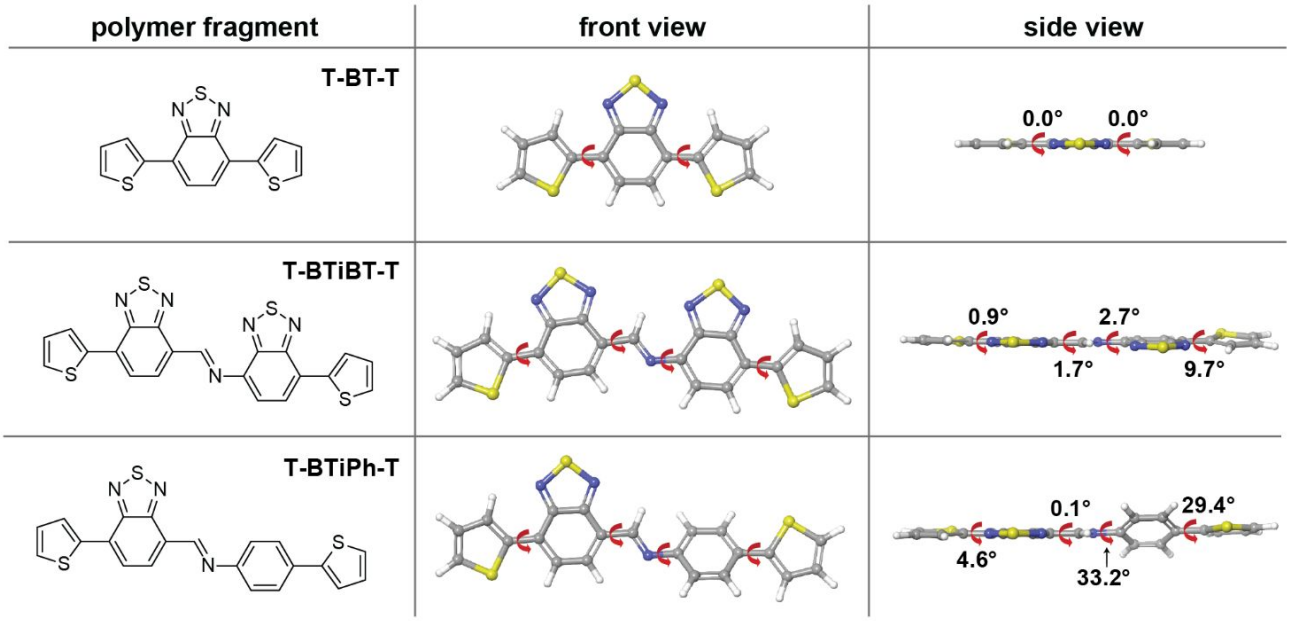

Figure 3. Chemical structures and corresponding DFT-optimized geometries of the BT and degradable BT units flanked by thiophenes (T). Dihedral angles are marked by red arrows in both the front and side view.

orbitals for T-BT-T and T-BTiBT-T show conjugation for charge transport is maintained along the polymer fragment backbone (Figure S20). However, due to backbone twisting, the calculations suggest the T-BTiPh-T fragment may not maintain good intrachain conjugation, which could affect the charge transport mechanism for pIDT-BTiPh (i.e., charge transfer through the BTiPh unit).

As the degradation of the polymers are monitored by UV-vis, UV-vis spectra were simulated for the degradation products of pIDT-BTiBT (optimized at the B3LYP-D3/6-31G** level) using TD-DFT at the CAM-B3LYP-D3/6-31G++** level (Figures S21-24). Using the experimental UV-vis spectrum for the synthesized dialdehyde-functionalized BT-IDT-BT in THF as a reference, we scaled the calculated UV-vis spectra and half-bandwidth of transitions accordingly (Figure S25). The overlaid spectra showed the lower energy transition for the aldehyde-amino-functionalized degradation product was red-shifted compared to the other two products likely due to introduced donor-acceptor behavior. Additionally, the diamino-functionalized product exhibited a notably stronger intensity and lower energy π–π* transition (at ~425 nm). We expect to observe a mixture of these absorption features from the degradation products of pIDT-BTiBT.

2.3. Optical, Morphological, and Mechanical Characterization

With the synthesized degradable IDT-based polymers and their calculated structural differences compared to nondegradable pIDT-BT, we characterized the optical and morphological properties in solution and as thin films. UV-vis of the polymers in both solution and thin films showed two main absorption peaks, with the lower energy transition resulting from internal charge transfer between the donor and acceptor units and a higher energy band at ~400 nm (Figure 4a,b).[31] In dilute chlorobenzene solution (0.01 mg/mL), pIDT-BTiBT and pIDT-10BTiPh, which only had ~10% mol BTiPh, exhibited peak broadening of the charge transfer band relative to pIDT-BT. We hypothesize this broadening could arise from increased regioirregularity and structural disorder from the BTiBT unit, leading to a variation of vibronic transition energies. The onset of absorption was slightly red-shifted, which suggests BTiBT is a stronger acceptor than BT as additional electron-withdrawing BT and imine units were introduced (i.e., energy required for internal charge transfer decreased). In contrast, pIDT-BTiPh was blue-shifted significantly (~50 nm) relative to pIDT-BT, which can be attributed to its more pronounced backbone twisting, disrupting conjugation along the polymer backbone. Similar trends were observed across common processing solvents (Figure S26). UV-vis spectra of the polymer thin films also showed similar trends as in solution with more distinct 0-0 transitions, corresponding to J-aggregation behavior, observed in the charge transfer band (Figure 4b and Figure S27).[32] pIDT-BT displayed the highest 0-0 to 0-1 peak ratio, indicative of highly ordered chains arising from its planar and rigid backbone.[33–37] The degradable IDT-based polymers all had similar 0-0 to 0-1 peak ratios, which were much less pronounced compared to pIDT-BT likely due to their deviations from backbone planarity and regioirregularity from their asymmetric imine units. It was noted that pIDT-10BTiPh showed more J-aggregation behavior than pIDT-BTiBT, which we attributed to increased M_n, and thus conjugation length, of the polymer.

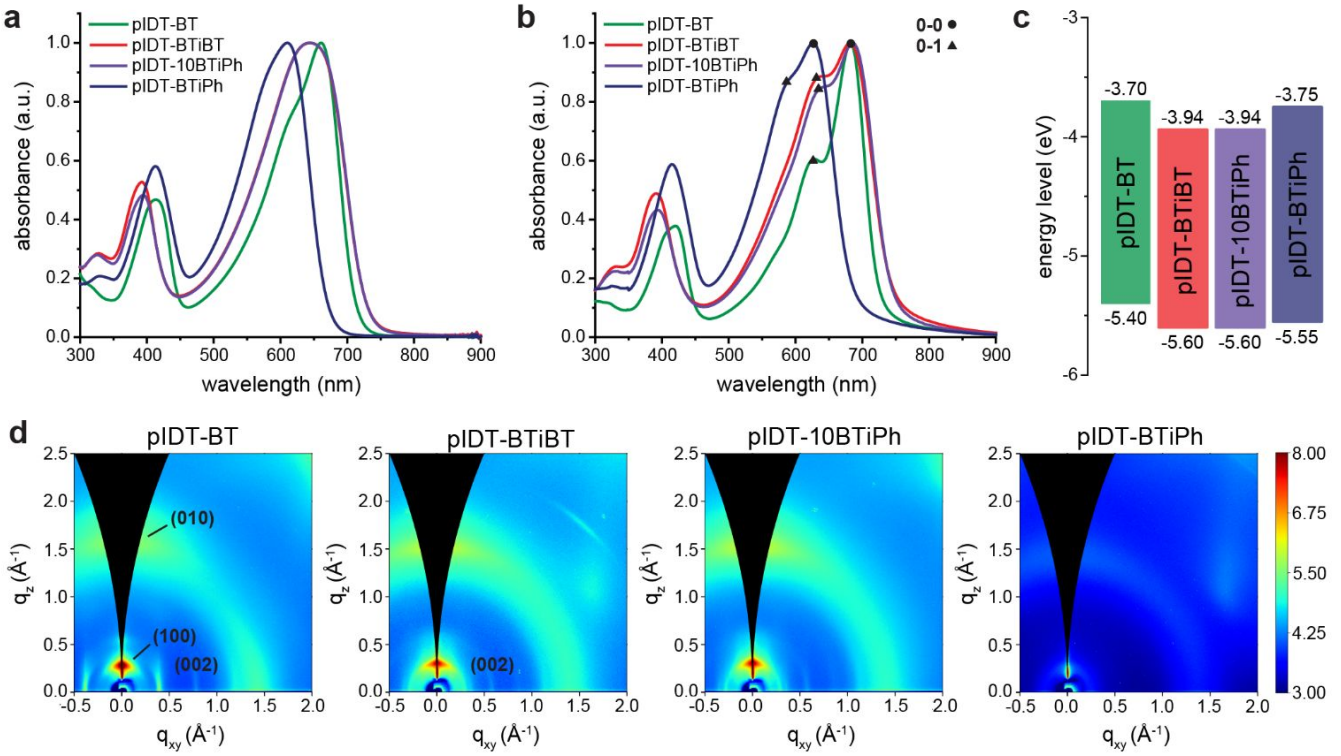

Figure 4. Optical and morphology property characterization. Normalized UV-vis absorption spectra of nondegradable and degradable IDT-based polymers in (a) chlorobenzene solution (0.01 mg/mL) at 25 °C and (b) annealed thin films spin-coated from chlorobenzene. (c) Representation of highest occupied molecular orbital (HOMO) and lowest unoccupied molecular orbital (LUMO) energy levels as well as band gap of four IDT-based polymers. (d) GIXD patterns of the annealed polymer thin films for the four IDT-based polymers.

Highest occupied molecular orbital (HOMO) energy levels were measured by PESA, and the optical band gaps were calculated from the onsets of absorption in annealed thin film UV-vis spectra to estimate the lowest unoccupied molecular orbital (LUMO) energy levels (Figure 4c). The results are summarized in Table S2. The HOMO energies for all degradable IDT-based polymers were deeper than that of pIDT-BT due to incorporation of the electron-withdrawing imine group, with pIDT-BTiBT and pIDT-10BTiPh being further lowered by the additional BT unit compared to pIDT-BTiPh.

We performed GIXD measurements of the annealed thin films to characterize the polymers' film morphology and crystallite packing. 2D GIXD patterns for the reference pIDT-BT and three degradable IDT-based polymers spin-coated and annealed on octadecyltrimethoxysilane (OTS)-modified Si wafers are shown in Figure 4d. Relevant plane spacings, full width half maxima (fwhm), and crystallite coherence length (CCL) are reported in Table 2 and Table S3.[38,39] The corresponding in-plane and out-of-plane scattering profiles are shown in Figure S28. Similar to pIDT-BT, both edge-on and face-on orientations were observed in pIDT-BTiBT and pIDT-10BTiPh films, with (100) and (200) lamellar stacking peaks as well as (010) π–π reflections in the out-of-plane direction.[18,19,21] The lamellar stacking peaks for pIDT-BTiBT and pIDT-10BTiPh were smaller than traditional pIDT-BT, likely due to a greater backbone:sidechain ratio or greater sidechain disorder. The (200) and (010) reflections are broad, indicative of small crystallite grain size or substantial cumulative lattice disorder.[39] It should be noted that due to the overlapping scattering along the q_z direction from the OTS surface modification as well as amorphous alkyl chains of the polymer, the π–π spacing extracted from the weak (010) diffraction peak could not be deconvoluted during fitting. The π–π spacing values generally agreed with DFT geometry calculations and thin film UV-vis absorption spectra, with pIDT-BT having the closest packing due to its extreme planarity and pIDT-BTiPh with the largest π–π spacing due to its significant backbone twisting. Along the q_{xy} direction, (00*l*) reflections were observed, corresponding to repeat unit length. Based on the (002) peaks, pIDT-BTiBT and pIDT-10BTiPh had larger spacing values for backbone periodicity relative to that of pIDT-BT which was expected from their larger repeat units. In contrast to the other IDT-based polymers, pIDT-BTiPh did not exhibit observable lamellar stacking and (00*l*) reflections, indicating the polymer film was much more amorphous.

Table 2. Relevant Peak Positions from GIXD

polymer	lamellar spacing (Å)[a]	π–π spacing (Å)[b]	backbone spacing (Å)[c]
pIDT-BTiBT	21.4	4.17	22.0
pIDT-10BTiPh	21.3	4.11	21.9
pIDT-BTiPh	-	4.41	-
pIDT-BT	22.9	4.01	16.1

[a]Extracted from fitting the (100) diffraction peak. [b]Extracted from fitting the (010) diffraction peak. [c]Extracted from fitting the (002) diffraction peak.

To further examine thin film morphology and mechanical properties, we conducted AFM-based nanomechanical

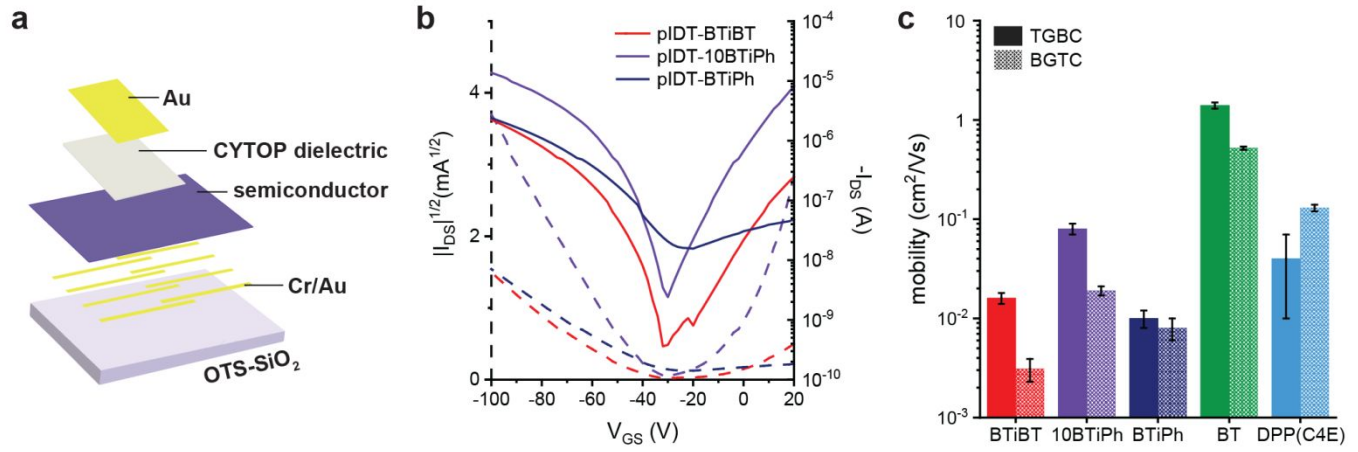

Figure 5. Electronic performance of FETs. (a) Top-gate bottom-contact (TGBC) device architecture. (b) Representative saturation transfer curves for degradable IDT-based polymers in TGBC device structure (V_{DS} = −100 V). The dashed lines correspond to the square root of the drain current. (c) Average charge carrier mobilities from six devices of the degradable IDT-based polymers and reference polymers in both TGBC and bottom-gate top-contact (BGTC) device architectures.

measurements. Height and Derjaguin-Muller-Toporov (DMT) modulus images are shown in Figures S29-30. All polymer films were smooth, with root mean square (RMS) roughness values below 1.7 nm. Large (>500 nm) aggregates were omitted from calculated RMS roughness values. As nanomechanical images of pDPP(C4E)-TIT had not been previously recorded, the semicrystalline polymer was also measured. The DMT modulus distributions displayed degradable IDT polymers were stiffer than both pIDT-BT and pDPP(C4E)-TIT, potentially due to a greater amount of rigid, conjugated regions compared to softer alkyl chains of the polymer.

Bulk mechanical properties of the thin films were investigated by transferring them onto polydimethylsiloxane (PDMS) elastomers for measurement of crack onset strain.[40] Optical microscope images of the polymer films under 0-100% strain are shown in Figure S31. We observed low crack onset strains of 20-40% for pIDT-BTiBT and pIDT-10BTiPh due to their low M_n and thus higher crystallinity. pIDT-BT, which had a higher M_n but greater rigidity, also showed a similar crack onset strain. On the other hand, highly disordered pIDT-BTiPh did not crack until 100% strain. Compared to semicrystalline pDPP(C4E)-TIT, which cracked around 40-60% strain, pIDT-BTiPh showed potential for advanced stretchability.

2.4. Electronic Performance of Field-Effect Transistors

We fabricated top-gate bottom-contact (TGBC) and bottom-gate top-contact (BGTC) field effect transistors (FETs) to measure the charge carrier mobilities of the degradable IDT-based polymer semiconductors. Detailed fabrication procedures are described in the Supporting Information. Representative transfer curves for TGBC devices operated in the saturation regime are depicted in Figure 5a-b and Figure S32. Output curves and BGTC transfer curves are shown in Figures S33-34. The average mobilities and performance metrics are summarized in Figure 5c and Tables S4-5. All IDT-based polymers displayed better performance in the TGBC configuration using CYTOP as the dielectric as they were previously hypothesized to have a more favorable dielectric-semiconductor interface with nonpolar polymer dielectrics.[21] TGBC FETs exhibited ambipolar charge transport under nitrogen, promoted by encapsulation from the CYTOP dielectric, with dominant p-type behavior. pIDT-BT displayed the highest saturation hole mobilities (μ_{sat}), while the degradable IDT-based polymers all displayed reduced μ_{sat}, which we attributed to increased disorder in the polymer backbones as shown by DFT calculations and GIXD measurements. Of the degradable IDT-based polymers, pIDT-10BTiPh exhibited the highest μ_{sat}, which can be ascribed to increased aggregation and reduced π–π spacing observed in thin film UV-vis and GIXD experiments, respectively. pIDT-10BTiPh displayed comparable mobilities to semicrystalline pDPP(C4E)-TIT.

2.5. Degradation Studies

To monitor the degradation of the imine-based semiconducting polymers in solution (Figure S35), we used UV-vis, GPC, and NMR techniques. For UV-vis and GPC experiments, a 150-fold molar excess of trifluoroacetic acid (TFA) and water were added to a dilute polymer solution (~0.01 mg/mL) using common thin film processing solvents. Representative UV-vis spectra of the degradation of pIDT-BTiBT in THF at room temperature is shown in Figure 6a. A similar method as previously used in literature was used to quantify the degradation of the different classes of polymers, in which the absorbance at λ_{max} was tracked over time.[6] However, unlike DPP-based monomers, IDT-based monomers did not undergo ring-opening under acidic conditions. Therefore, the absorbance at λ_{max} did not go to zero when the polymer solution reached equilibrium after addition of acid and water. The absorption spectrum at equilibrium overlapped well with the experimental spectrum of the synthesized dialdehyde-functionalized BT-IDT-BT in THF and simulated TD-DFT UV-vis spectra of the monomeric degradation products (Figures S25 and S36), indicating the equilibrium degradation mixture consisted of primarily monomeric units. For the degradable IDT-based polymers, the final absorbance at λ_{max} was subtracted from the initial absorbance at λ_{max} to give the allowed degradation range. The final absorbance was again subtracted from the absorbance at each timepoint and then normalized over this allowed degradation range for comparison over time. The degradation in solution of the nanocrystalline, imine-based IDT polymers was orders of magnitude faster than previous studies of degradable, semicrystalline DPP-based polymers even at seven times less concentrated acidic conditions (Figures 6b-c and S37).[6] The degradable IDT-based polymers degraded within two hours

compared to pDPP(C4E)-TIT, which was unchanged on this timescale as it previously took days for degradation. Similar trends were observed in chlorinated solvents; however, due to acid-doping of IDT-based polymers facilitated by these solvents, it was difficult to decouple degradation from acid-doping for quantification of timescale comparisons (Figures S38-39).[41–43] In toluene solution, doping behavior was not observed on short timescales (< 1 day), and the degradable IDT-based polymers were measured to have completely degraded within only 5 min. (Figure S40). In addition to accelerated degradation arising from structural effects and decreased aggregation of the IDT-based polymers, we ascribe the faster degradation rates to the electronic effects of the BT-based imine bonds which are more susceptible to hydrolysis relative to that of pDPP(C4E)-TIT (Figure S41).[44,45]

To confirm degradation into mainly monomeric units, we used GPC to measure the M_n of polymers before and after degradation in dilute THF solution with a 150-fold molar excess of TFA and water. GPC traces displayed the degradation products were primarily monomeric after two days as they overlapped well with the model degradation compound (Figures 6d and S42). At the molecular scale, in situ NMR degradation experiments were conducted at a higher concentration of polymer solution in THF (~5 mg/mL) using the same molar excess of deuterated TFA and water. We observed degradation within 3 h, as seen by the disappearance of the imine peak (Figures 6e and S43). Additionally, the broad polymer peaks became sharper ones that corresponded to that of the monomeric degradation compound. Due to the overlapping of the aldehyde peaks with the peroxides in deuterated THF,[46] the new aldehyde peaks at 10.8 ppm were partially obscured in the polymer degradation products and model compound.

For examination of degradation in the thin film, we first conducted thickness and contact angle measurements of the polymer films. The films were processed to have similar thicknesses of around 70 nm for proper comparison in degradation studies (Table S6). All of the IDT-based polymers were more hydrophobic than the semicrystalline DPP-based polymer with hydrophilic sidechains (Figures 6f and S44 and Table S7). Additionally, in situ QCM experiments were performed to examine water diffusion kinetics and swelling behavior of the thin films. Agreeing with contact angle measurements, hydrophilic pDPP(C4E)-TIT demonstrated more swelling by water compared to the degradable IDT-based polymers (Figure 6g).

To measure degradation of the thin films by UV-vis, we used our previously developed method of transferring the film onto an adhesive, optically clear PDMS substrate and soaking in acidic aqueous solution at 70 °C.[6] The degradation was quantified using the same process as for solution UV-vis degradation studies. Similar trends were observed in the thin film as in solution, where all degradable polymers lacking long-range order degraded much faster than the semicrystalline reference polymer. We attributed the accelerated degradation to decreased aggregation and increased π–π spacing, derived from structural regioirregularity, of the IDT-based polymers as observed by thin film UV-vis and GIXD measurements.[6] In organic acid, degradation was rapid, with all imine-based IDT polymers reaching complete degradation within one week (Figures 6h and S45). Unlike in solution, pDPP(C4E)-TIT exhibited noticeable degradation during these timescales as it enabled better diffusion of the aqueous degradation solution into the film compared to the more hydrophobic IDT-based polymers. The absorbance of nondegradable pIDT-BT stayed fairly constant, with a slight decrease observed potentially from physical abrasion over time. Additionally, the degradable IDT-based polymers degraded within 80 days under milder acidic conditions of 0.1 M hydrochloric acid (HCl), resembling stomach acid in the human body (Figures 6i-j and S46). As HCl was an aqueous acid, the diffusion was much slower, and hence, degradation occurred over a longer timescale. We also monitored degradation by QCM under a constant flow (50 μL/min) of 0.1 M HCl at 65 °C. We observed faster degradation kinetics and mass loss for the degradable IDT-based polymers relative to pDPP(C4E)-TIT despite being swelled less by aqueous solution (Figure S47), demonstrating polymer morphology and aggregation may have a greater impact on degradation timescales than hydrophilicity. Even among the degradable IDT-based polymers, pIDT-BTiPh films displayed a slightly faster degradation rate, demonstrating the delicate balance needed in designing less ordered polymer morphologies and their resulting mechanical, electronic, and degradation properties. These studies show that polymers lacking long-range order have the potential to be degraded in more biologically-relevant environments. A design strategy that targets improved penetration of degradation solution into the film through both reduced aggregation and hydrophilic groups would potentially allow for even milder conditions to be used. Unlike the previous sidechain study of semicrystalline pDPP-TIT, where electronic performance was inversely correlated to degradation time (i.e., highest performing semiconductors degraded the slowest),[6] the polymers with short-range order underwent rapid degradation despite similar electronic performance to the semicrystalline reference polymer.

3. Conclusion

In summary, we synthesized a new class of degradable imine-based semiconducting polymers with "disordered" morphologies and characterized these polymers' mechanical, electronic, and degradation properties. The polymers were synthesized via Suzuki couplings, eliminating the use of toxic tin reagents commonly used in polymer semiconductor syntheses. Additionally, the regioirregularity and disorder introduced by backbone twisting led to increased stretchability for future implantables and wearables. The IDT-based polymers with short-range order exhibited similar charge carrier mobilities to their semicrystalline counterpart pDPP(C4E)-TIT with long-range order but degraded orders of magnitude faster in both solution and thin film under less harsh acidic conditions. These degradable, nanocrystalline polymers push the boundaries of degradation timescales accessible within classes of semiconducting polymers, suggesting promise for technologies with triggerable or on-demand degradation. Future work on expanding the biocompatibility of such semiconducting polymers is crucial for the integration of transient devices with the human body and environment.

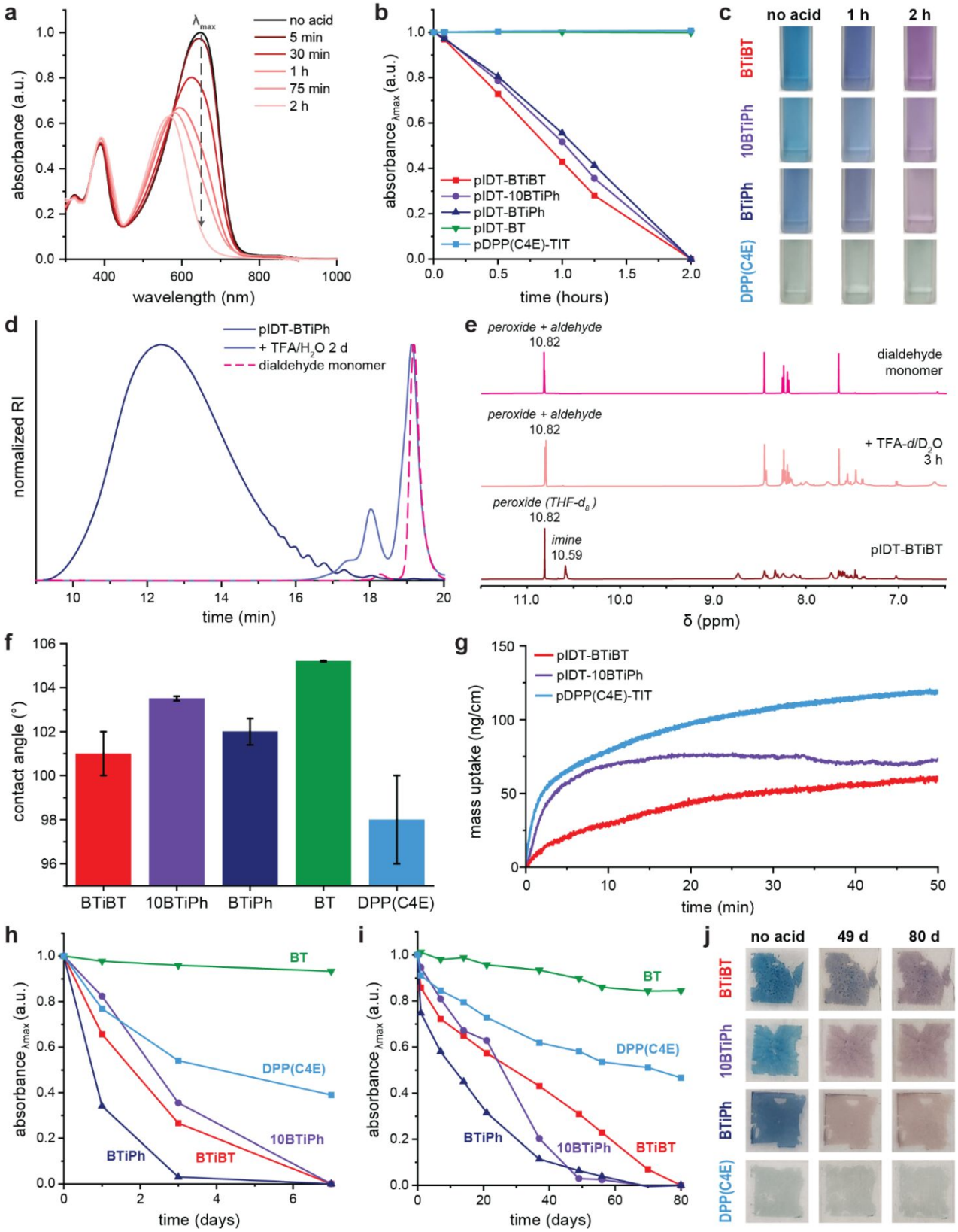

Figure 6. Solution and thin film degradation studies. (a) UV-vis spectra of pIDT-BTiBT in THF (~0.01 mg/mL) following the addition of TFA and water. (b) UV-vis absorption intensities at λ_{max} plotted over time for degradation of all polymers in THF. (c) Color change over time for the degradation of polymers in THF. (d) GPC chromatograms of pIDT-BTiPh before and after degradation in THF (~0.01 mg/mL) compared to that of the model degradation compound. (e) NMR spectra demonstrating the cleavage of imine bonds in THF (~5 mg/mL) after addition of TFA and water, with the degradation product resembling the model compound. (f) Contact angles of the IDT-based polymer films compared with pDPP(C4E)-TIT. (g) Water diffusion kinetics by QCM of degradable IDT-based polymers compared with pDPP(C4E)-TIT. (h) UV-vis absorption intensities at λ_{max} plotted over time for degradation of polymer thin films in 0.5 M TFA and (i) 0.1 M HCl. (j) Color change over time for the degradation of polymer thin films in 0.1 M HCl.

Conflicts of interest

There are no conflicts to declare.

Acknowledgements

J.A.C. is supported by the Department of Defense (DoD) through the National Defense Science & Engineering Graduate (NDSEG) Fellowship Program and the Stanford Enhancing Diversity in Graduate Education Doctoral Fellowship Program. L.M. acknowledges funding through the Walter Benjamin Fellowship Program by the Deutsche Forschungsgemeinschaft (DFG 456522816). A.E.P.-A. acknowledges support from the National Science Foundation Graduate Research Fellowship Program under Grant No. DGE-1656518, the Stanford Knight–Hennessy Scholarship, and the Stanford Enhancing Diversity in Graduate Education Doctoral Fellowship. X.J. is supported by the American Association of University Women through International Fellowship. The DFT and TD-DFT calculations for this project were performed on the Sherlock cluster. We would like to thank Stanford University and the Stanford Research Computing Center for providing computational resources and support that contributed to these research results. The authors acknowledge the use of the Stanford Synchrotron Radiation Lightsource, SLAC National Accelerator Laboratory, which is supported by the U.S. Department of Energy, Office of Science, Office of Basic Energy Sciences under Contract No. DE-AC02-76SF00515. This work was in part supported by the Stanford Precourt Pioneering Project - "Reinventing Plastics." Part of this work was performed at the Stanford Nano Shared Facilities (SNSF), supported by the National Science Foundation under award ECCS-2026822, as well as the Medicinal Chemistry Knowledge Center (MCKC), supported by the NIH High End Instrumentation Grant 1 S10 OD028697-01. We would like to thank Ashley M. Robinson, Yuran Shi, Qianhe (Kelly) Liu, Hao-Wen Cheng, Song Zhang, and Yilei Wu for assistance with instrumentation and helpful discussions.

References

1 T. Lei, M. Guan, J. Liu, H.-C. Lin, R. Pfattner, L. Shaw, A. F. McGuire, T.-C. Huang, L. Shao, K.-T. Cheng, J. B.-H. Tok and Z. Bao, *PNAS*, 2017, **114**, 5107–5112.

2 H. Tran, V. R. Feig, K. Liu, H.-C. Wu, R. Chen, J. Xu, K. Deisseroth and Z. Bao, *ACS Cent. Sci.*, 2019, **5**, 1884–1891.

3 H. Tran, S. Nikzad, J. A. Chiong, N. J. Schuster, A. E. Peña-Alcántara, V. R. Feig, Y.-Q. Zheng and Z. Bao, *Chem. Mater.*, 2021, **33**, 7465–7474.

4 J. A. Chiong, H. Tran, Y. Lin, Y. Zheng and Z. Bao, *Advanced Science*, 2021, **8**, 2101233.

5 H. Park, Y. Kim, D. Kim, S. Lee, F. S. Kim and B. J. Kim, *Advanced Functional Materials*, 2022, **32**, 2106977.

6 J. A. Chiong, Y. Zheng, S. Zhang, G. Ma, Y. Wu, G. Ngaruka, Y. Lin, X. Gu and Z. Bao, *J. Am. Chem. Soc.*, 2022, **144**, 3717–3726.

7 A. Uva, A. Lin and H. Tran, *J. Am. Chem. Soc.*, , DOI:10.1021/jacs.2c12668.

8 K. K. Fu, Z. Wang, J. Dai, M. Carter and L. Hu, *Chem. Mater.*, 2016, **28**, 3527–3539.

9 C. M. Boutry, L. Beker, Y. Kaizawa, C. Vassos, H. Tran, A. C. Hinckley, R. Pfattner, S. Niu, J. Li, J. Claverie, Z. Wang, J. Chang, P. M. Fox and Z. Bao, *Nature Biomedical Engineering*, 2019, **3**, 47–57.

10 N. Bokka, V. Selamneni and P. Sahatiya, *Materials Advances*, 2020, **1**, 2818–2830.

11 M. J. Tan, C. Owh, P. L. Chee, A. K. K. Kyaw, D. Kai and X. J. Loh, *J. Mater. Chem. C*, 2016, **4**, 5531–5558.

12 V. R. Feig, H. Tran and Z. Bao, *ACS Cent. Sci.*, 2018, **4**, 337–348.

13 J. Lee, B. Yoo, H. Lee, G. D. Cha, H.-S. Lee, Y. Cho, S. Y. Kim, H. Seo, W. Lee, D. Son, M. Kang, H. M. Kim, Y. I. Park, T. Hyeon and D.-H. Kim, *Advanced Materials*, 2017, **29**, 1603169.

14 A. Gumus, A. Alam, A. M. Hussain, K. Mishra, I. Wicaksono, G. A. Torres Sevilla, S. F. Shaikh, M. Diaz, S. Velling, M. T. Ghoneim, S. M. Ahmed and M. M. Hussain, *Advanced Materials Technologies*, 2017, **2**, 1600264.

15 G. Chen, L. Xu, P. Zhang, B. Chen, G. Wang, J. Ji, X. Pu and Z. L. Wang, *Advanced Materials Technologies*, 2020, **5**, 2000455.

16 Y. Gao, Y. Zhang, X. Wang, K. Sim, J. Liu, J. Chen, X. Feng, H. Xu and C. Yu, *Science Advances*, 2017, **3**, e1701222.

17 S.-K. Kang, L. Yin and C. Bettinger, *MRS Bulletin*, 2020, **45**, 87–95.

18 W. Zhang, J. Smith, S. E. Watkins, R. Gysel, M. McGehee, A. Salleo, J. Kirkpatrick, S. Ashraf, T. Anthopoulos, M. Heeney and I. McCulloch, *J. Am. Chem. Soc.*, 2010, **132**, 11437–11439.

19 X. Zhang, H. Bronstein, A. J. Kronemeijer, J. Smith, Y. Kim, R. J. Kline, L. J. Richter, T. D. Anthopoulos, H. Sirringhaus, K. Song, M. Heeney, W. Zhang, I. McCulloch and D. M. DeLongchamp, *Nat Commun*, 2013, **4**, 2238.

20 D. Venkateshvaran, M. Nikolka, A. Sadhanala, V. Lemaur, M. Zelazny, M. Kepa, M. Hurhangee, A. J. Kronemeijer, V. Pecunia, I. Nasrallah, I. Romanov, K. Broch, I. McCulloch, D. Emin, Y. Olivier, J. Cornil, D. Beljonne and H. Sirringhaus, *Nature*, 2014, **515**, 384–388.

21 Y. Zheng, G.-J. N. Wang, J. Kang, M. Nikolka, H.-C. Wu, H. Tran, S. Zhang, H. Yan, H. Chen, P. Y. Yuen, J. Mun, R. H. Dauskardt, I. McCulloch, J. B.-H. Tok, X. Gu and Z. Bao, *Advanced Functional Materials*, 2019, **29**, 1905340.

22 H. Bronstein, D. S. Leem, R. Hamilton, P. Woebkenberg, S. King, W. Zhang, R. S. Ashraf, M. Heeney, T. D. Anthopoulos, J. de Mello and I. McCulloch, *Macromolecules*, 2011, **44**, 6649–6652.

23 M. Nikolka, M. Hurhangee, A. Sadhanala, H. Chen, I. McCulloch and H. Sirringhaus, *Advanced Electronic Materials*, 2018, **4**, 1700410.

24 A. Wadsworth, H. Chen, K. J. Thorley, C. Cendra, M. Nikolka, H. Bristow, M. Moser, A. Salleo, T. D. Anthopoulos, H. Sirringhaus and I. McCulloch, *J. Am. Chem. Soc.*, 2020, **142**, 652–664.

25 V. Lemaur, J. Cornil, R. Lazzaroni, H. Sirringhaus, D. Beljonne and Y. Olivier, *Chem. Mater.*, 2019, **31**, 6889–6899.

26 C. Cendra, L. Balhorn, W. Zhang, K. O'Hara, K. Bruening, C. J. Tassone, H.-G. Steinrück, M. Liang, M. F. Toney, I. McCulloch, M. L. Chabinyc, A. Salleo and C. J. Takacs, *ACS Macro Lett.*, 2021, **10**, 1306–1314.

27 B. Zhao, D. Pei, Y. Jiang, Z. Wang, C. An, Y. Deng, Z. Ma, Y. Han and Y. Geng, *Macromolecules*, 2021, **54**, 9896–9905.

28 S. L. Shenoy, W. D. Bates, H. L. Frisch and G. E. Wnek, *Polymer*, 2005, **46**, 3372–3384.

29 H. Ren, J. Zhang, Y. Tong, J. Zhang, X. Zhao, N. Cui, Y. Li, X. Ye, Q. Tang and Y. Liu, *J. Mater. Chem. C*, 2020, **8**, 15646–15654.

30 H. Chen, A. Wadsworth, C. Ma, A. Nanni, W. Zhang, M. Nikolka, A. M. T. Luci, L. M. A. Perdigão, K. J. Thorley, C. Cendra, B. Larson, G. Rumbles, T. D. Anthopoulos, A. Salleo, G. Costantini, H. Sirringhaus and I. McCulloch, *J. Am. Chem. Soc.*, 2019, **141**, 18806–18813.
31 B. C. Schroeder, Z. Huang, R. S. Ashraf, J. Smith, P. D'Angelo, S. E. Watkins, T. D. Anthopoulos, J. R. Durrant and I. McCulloch, *Advanced Functional Materials*, 2012, **22**, 1663–1670.
32 T. Eder, T. Stangl, M. Gmelch, K. Remmerssen, D. Laux, S. Höger, J. M. Lupton and J. Vogelsang, *Nat Commun*, 2017, **8**, 1641.
33 P. J. W. Sommerville, A. H. Balzer, G. Lecroy, L. Guio, Y. Wang, J. W. Onorato, N. A. Kukhta, X. Gu, A. Salleo, N. Stingelin and C. K. Luscombe, *ACS Polym. Au*, 2023, **3**, 59–69.
34 S. Wood, J. Wade, M. Shahid, E. Collado-Fregoso, D. D. C. Bradley, J. R. Durrant, M. Heeney and J.-S. Kim, *Energy Environ. Sci.*, 2015, **8**, 3222–3232.
35 T. Sarkar, S. A. Schneider, G. Ankonina, A. D. Hendsbee, Y. Li, M. F. Toney and G. L. Frey, *Chem. Mater.*, 2020, **32**, 7338–7346.
36 P. J. W. Sommerville, Y. Li, B. X. Dong, Y. Zhang, J. W. Onorato, W. K. Tatum, A. H. Balzer, N. Stingelin, S. N. Patel, P. F. Nealey and C. K. Luscombe, *Macromolecules*, 2020, **53**, 7511–7518.
37 Y. Li, W. K. Tatum, J. W. Onorato, Y. Zhang and C. K. Luscombe, *Macromolecules*, 2018, **51**, 6352–6358.
38 D.-M. Smilgies, *J Appl Cryst*, 2009, **42**, 1030–1034.
39 J. Rivnay, S. C. B. Mannsfeld, C. E. Miller, A. Salleo and M. F. Toney, *Chem. Rev.*, 2012, **112**, 5488–5519.
40 N. Balar and B. T. O'Connor, *Macromolecules*, 2017, **50**, 8611–8618.
41 Y. Liu, B. Zhao, J. Liu, Z. Wang, Z. Liang, W. Dong, C. Xu, B. Wang, Z. Fei and Y. Han, *ACS Appl. Polym. Mater.*, 2022, **4**, 3877–3884.
42 J. Byeon, D. Kim, M. Kyeong, I. G. Bak and S. Hong, *Chem. Mater.*, 2023, **35**, 2133–2145.
43 T. Liu, D. Xie, J. Xu and C. Pan, *Polymers*, 2020, **12**, 1463.
44 E. H. Cordes and W. P. Jencks, *J. Am. Chem. Soc.*, 1963, **85**, 2843–2848.
45 H. Celik, J. Ludvik and P. Zuman, *Electrochimica Acta*, 2006, **51**, 5845–5852.
46 P. J. M. Stals, M. A. J. Gillissen, R. Nicolaÿ, A. R. A. Palmans and E. W. Meijer, *Polymer Chemistry*, 2013, **4**, 2584–2597.